

Nonlinear Optical Probe of Indirect Excitons

A. V. Nalitov,¹ M. Vladimirova,² A. V. Kavokin,^{3,4} L. V. Butov,⁵ and N. A. Gippius^{1,6}

¹*Institut Pascal, PHOTON-N2, Clermont Université, Blaise Pascal University, CNRS, 24 avenue des Landais, 63177 Aubière Cedex, France.*

²*Laboratoire Charles Coulomb, UMR 5221 CNRS/UM2, Université Montpellier 2, Place Eugene Bataillon, 34095 Montpellier Cedex 05, France*

³*School of Physics and Astronomy, University of Southampton, Southampton, SO17 1BJ, United Kingdom*

⁴*Spin Optics Laboratory, St-Petersburg State University, 1, Ulianovskaya, St-Petersburg, 198504, Russia*

⁵*Department of Physics, University of California at San Diego, La Jolla, California 92093-0319, USA*

⁶*A. M. Prokhorov General Physics Institute, RAS, Vavilova Street 38, Moscow 119991, Russia*

We propose the application of nonlinear optics for studies of spatially indirect excitons in coupled quantum wells. We demonstrate, that despite their vanishing oscillator strength, indirect excitons can strongly contribute to the photoinduced reflectivity and Kerr rotation. This phenomenon is governed by the interaction between direct and indirect excitons. Both dark and bright states of indirect excitons can be probed by these nonlinear optical techniques.

PACS numbers: 78.20.Bh, 78.67.De, 71.35.-y, 78.47.jg, 78.66.Fd

I. INTRODUCTION.

Studies of spatially indirect excitons (IX) in semiconductors have attracted considerable research efforts since early 1960's, fueled by the prediction of the remarkable quantum properties. This resulted in recent demonstration of quantum coherent effects including spontaneous coherence [1–3], long-range spin currents and associated polarization textures [4, 5] of indirect excitons. An IX can be formed by an electron and a hole confined in separate coupled quantum wells (CQW). Application of the electric field across the CQWs bends the band structure so that the IX state became the ground state of the system [6, 7]. The spatial separation of electrons and holes within IX allows them to achieve long lifetimes, which may be orders of magnitude longer than the lifetimes of spatially direct excitons (DX). At the same time, the spatial separation of electrons and holes strongly reduces the oscillator strength of IXs, with respect to DXs. This determines the choice of the experimental methods for studies of these quasiparticles. The most frequently used optical methods are based on the emission (photoluminescence, PL) spectroscopy. The PL signal scales linearly with the emission rate in time-resolved experiments and is nearly independent on the emission rate in cw experiments for the samples with low nonradiative recombination. A set of the linear optics methods was employed for studies of IXs, including the imaging spectroscopy [8], the time-resolved imaging [9], the polarization-resolved imaging [4], and the first-order coherence measurements [1–3]. However, the powerful methods of nonlinear optics, which have been successfully applied for DXs in quantum wells (QW) [10], [11] remain unexplored in the studies of IXs.

A nonlinear optical process, in its broadest definition, is a process in which the optical properties of the medium depend on the light field itself [12]. In the case of optical

pumping in semiconductors, light-induced modifications of the optical properties of the medium can persist for a long time after the perturbing light is turned off. In this case, a pump-probe arrangement can be used, with pump and probe interactions separated in time [13]. This allows for time-resolved studies of optical and spin coherence in the medium. In semiconductor QWs resonant optical pumping of DX resonance with circularly polarized light, and subsequent detection of the pump-induced dispersive response is widely used to study exciton population and spin dynamics [14]. Experimentally, either modification of intensity (photoinduced reflectivity) or the rotation of the polarization plane of the linearly polarized probe pulse (photoinduced Kerr rotation) upon reflection from the sample are measured [15]. These signals are proportional to the square of the oscillator strength of the excitonic transition and have a pronounced resonant character [12]. Thus, because the oscillator strength of IX is orders of magnitude lower than for DX, it is impossible to simply transpose the ideas developed for nonlinear spectroscopy of DX to IX.

In this paper, we show how IXs, despite their vanishing oscillator strengths, can induce measurable photoinduced reflectivity and Kerr rotation. Our proposal relies on two peculiar properties of the CQW structures. The first essential property is the spin conserving tunneling of electrons between the QWs [16]. It allows for substantial spin polarization of IX via optical orientation of DXs. This has been unambiguously demonstrated by polarization-resolved photoluminescence experiments [17]. Thus, optical pumping of IXs can be realized via the DX state. The second important effect is the spin-dependent coupling between DX and IX states. This coupling is quite strong in CQW, where each IX and each DX have either holes or electrons located in the same QW. This is why the presence of IX population in the structure alters DX resonance properties, mainly

via spin-dependent exchange interactions [42]. Therefore, we suggest that the detection of IX population and spin polarization can also be realized by exploiting the DX resonance. The Kerr rotation measured at the DX resonance is a sensitive method to access populations and spin polarizations of both bright and dark IX states. It may be used, in particular, for studies of dark excitons which strongly affect spin properties of excitonic condensates [4, 5, 18, 25]. We study the effect of DX-IX interaction quantitatively, calculating the spin-dependent shifts of the DX resonances in the presence of spin-polarized gas of IXs within Hartree-Fock and effective mass approximation. A phenomenological model based on non-local dielectric response model predicts the spectral dependence of photoinduced Kerr rotation and reflectivity induced by IXs and allows to analyze the impact of bright and dark IXs and DXs on these spectra. We also apply spin density matrix formalism to describe the dynamics of pump-probe signal in a realistic CQW structure.

This paper is organised as follows. In Section II we describe phenomenologically the spectral dependence of the reflectivity and Kerr rotation induced by spin-polarized IXs in the vicinity of DX resonance. Section III is devoted to the explicit calculation DX-IX and IX-IX interaction energies. In Section IV we formulate the spin density matrix model of excitons in CQWs. It accounts for optical generation of DX excitons, tunneling between the QWs and spin relaxation. We use the basis of 16 exciton states (both DX and IX have four possible spin projections on the growth axis) and calculate typical reflectivity and Kerr rotation signals as a function of delay between pump and probe pulses. Section V summarizes and concludes the paper.

II. PHENOMENOLOGICAL MODEL.

In this Section we analyse phenomenologically the effect of the IX population in the CQW structure on the polarization and intensity of the linearly polarized weak probe wave, resonant with the DX transition. Let us consider a CQW structure schematically shown in Figure 1. It consists of two QWs, separated by a potential barrier of the width d and covered by a thick barrier layer of the width l . A static electric field is applied along the z -axis, perpendicular to the CQW plane. Two optically-active ground DX levels in this system with total spin ± 1 are denoted as E_e and E_h , and the corresponding wavefunctions as Ψ_e and Ψ_h , respectively [43]. Hereafter, the indices e (h) denote the QW where electrons (holes) are driven by the static gate voltage. In the case of two identical quantum wells, DX levels split into symmetrical and antisymmetrical states with very small energy difference [6] that we will ignore here and assume $E_e = E_h$.

The electric field of the incident probe beam can be written as $\mathbf{E} = \mathbf{e}_x E_0 e^{i(kz - \omega t)}$. Here we consider the nor-

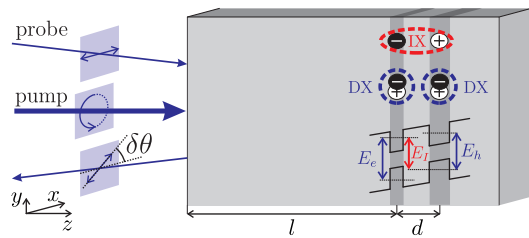


FIG. 1: Sketch of pump-probe experiment on CQWs sample. DX and IX optical transitions are shown. Both pump and probe frequencies are resonant with one of DX resonance.

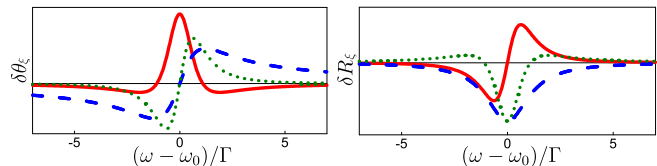


FIG. 2: Kerr rotation ($\delta\theta_\xi$) and photoinduced reflectivity (δR_ξ) spectra, calculated from Eq. (6) assuming different nonlinearities: DX energy shift ($\xi = \omega_0$, red solid line), DX transition saturation ($\xi = \Gamma_0$, blue dashed line) and DX non-radiative broadening ($\xi = \Gamma$, green dotted line).

mally incident probe beam characterized by the wavevector k , propagating along z -axis and linearly polarized along the x axis. The amplitude reflection coefficient from QW for such wave in the vicinity of one of DX transition frequencies $\omega_0 = E_{e(h)}/\hbar$ is related to the exciton wavefunction $\Psi = \Psi_{e(h)}(\boldsymbol{\rho}, z_{el}, z_{hh})$ by a textbook formula [19, 20] taken in the limit of $kd \ll 1$:

$$r_{\text{QW}}(\omega) = \frac{i\Gamma_0}{\omega_0 - \omega - i(\Gamma_0 + \Gamma)}, \quad (1)$$

where the radiative decay rate is given in

$$\Gamma_0 = \frac{\pi}{2} k \omega_{LT} a_B^3 S \left[\int \Psi(\boldsymbol{\rho} = 0, z, z) dz \right]^2, \quad (2)$$

ω_{LT} is the longitudinal-transverse splitting, a_B is the bulk exciton Bohr radius, S is the sample normalization area, and Γ is the exciton non-radiative decay rate, $\boldsymbol{\rho}$ is the in-plane separation of electron and hole, $z_{el(hh)}$ are electron (hole) z coordinates.

In the most experimentally relevant case $|r_{\text{QW}}(\omega)| \ll 1$. Taking into account the interference between waves reflected from the surface of the cap layer having a refractive index n and those reflected from CQWs, neglecting re-reflections and reflections from deeper layers of the structure, the total reflectivity coefficient is

$$r = \frac{1-n}{1+n} + e^{2ikl} \frac{4n}{(n+1)^2} r_{\text{QW}}. \quad (3)$$

The presence of IXs can affect the DX transition parameters ω_0 , Γ_0 and Γ through various mechanisms.

Spin-dependent Coulomb interactions between IXs and DXs leads to the blue shift of DX levels and, in the case when IXs are polarized, their spin-splitting. IXs also saturate DX transitions due to the phase space filling effect, since IXs consist of electrons and holes in the same QWs as DXs. This effect is again spin-dependent. Finally, IXs may affect the non-radiative decay of DXs through the scattering processes involving spin-dependent transitions between DX and IX levels, or by screening the disorder potential. The renormalisation of exciton resonance frequencies and spin-splittings due to these interactions is responsible for the modulation of reflectivity and Kerr rotation spectra [44]. Indeed, all the interaction effects listed above can be accounted for by correcting the reflection coefficients for two circularly polarized components of the probe pulse, σ^\pm :

$$\delta r^\pm = \frac{\partial r}{\partial \omega_0} \delta \omega_0^\pm + \frac{\partial r}{\partial \Gamma_0} \delta \Gamma_0^\pm + \frac{\partial r}{\partial \Gamma} \delta \Gamma^\pm \quad (4)$$

The electric field of the reflected probe wave can be expressed in terms of these corrections as

$$\mathbf{E}_r = E_0 \frac{1}{\sqrt{2}} [(r + \delta r^+) \mathbf{e}_+ + (r + \delta r^-) \mathbf{e}_-] e^{i(kz - \omega t)}.$$

Here the basis of right and left circularly polarized waves $\mathbf{e}_\pm = (\mathbf{e}_x \pm i\mathbf{e}_y)/\sqrt{2}$ is used. One can see, that in the most general case, the corrections of the reflection coefficient may induce (i) circular dichroism, which leads to the build up of circular polarization, (ii) circular birefringence, which leads to the rotation of the polarization plane, or Kerr rotation, and (iii) modification of the probe intensity. In the limit of $|\delta r^\pm| \ll |r_{\text{QW}}| \ll 1$ Kerr rotation angle is linear in $(\delta r^+ - \delta r^-)$ [21], while photoinduced reflectivity is linear in $(\delta r^+ + \delta r^-)$:

$$\delta \theta = -\text{Im} \left\{ \frac{\delta r^+ - \delta r^-}{2r} \right\}, \quad \delta R = |r|^2 \text{Re} \left\{ \frac{\delta r^+ + \delta r^-}{r} \right\}. \quad (5)$$

Substituting Eqs.(3, 4) into Eq.(5) we express the three contributions to the photoinduced Kerr rotation and reflectivity as a function of corresponding modification of the excitonic characteristic ξ , which spans over the resonant frequency, radiative and non-radiative decay rates $\xi = \omega_0, \Gamma_0, \Gamma$:

$$\begin{aligned} \delta \theta_\xi &= \frac{2n}{n^2 - 1} \text{Im} \left\{ e^{2ikl} \frac{\partial r_{\text{QW}}}{\partial \xi} \right\} (\delta \xi^+ - \delta \xi^-), \\ \delta R_\xi &= -\frac{4n(n-1)}{(n+1)^3} \text{Re} \left\{ e^{2ikl} \frac{\partial r_{\text{QW}}}{\partial \xi} \right\} (\delta \xi^+ + \delta \xi^-). \end{aligned} \quad (6)$$

Figure 2 shows the contributions of different mechanisms to photoinduced Kerr rotation and reflectivity spectra in the vicinity of the DX resonance, calculated using Eqs.(6), assuming $2kl \ll 1$ and $n > 1$, $\delta \omega_0^- = \delta \Gamma_0^- = \delta \Gamma^- = 0$, and normalized so that $\delta \omega_0^+/\Gamma = -\delta \Gamma_0^+/\Gamma_0 =$

$\delta \Gamma^+/\Gamma$. This corresponds to: blue shift of the DX energy $\delta \omega_0$ (red solid line), reduction of the DX oscillator strength $\delta \Gamma_0$ (blue dashed line) and enhancement of non-radiative decay of DX, $\delta \Gamma$ (green dotted line). One can see, that the spectral profiles are qualitatively different. Thus, measuring photoinduced spectra should make possible the identification of the underlying nonlinearity. Note also, that spectral shape depends on the value of the phase factor $2kl$ in the Eq. (6), so that $\delta \theta$ and δR transform as imaginary and real parts of a complex value between the braces.

The roadmap for the measurement of the pump-probe signal induced by IX and determination of the underlying nonlinearities can be as follows. First of all, in real time-resolved pump-probe experiments, one operates with short pulses of light rather than with monochromatic waves. Therefore, to measure spectral dependence of the nonlinear signal the probe spectral width must be smaller than the DX linewidth $(\Gamma + \Gamma_0)$, which is accessible experimentally [22]. Second, one should avoid any contribution of DX population to the nonlinear signal. This can be easily realized by setting the delay between pump and probe pulses sufficiently long, because DX lifetime does not exceed 500 ps, while IX lifetime is at least an order of magnitude longer. Finally, fitting the measured pump-induced reflectivity and Kerr rotation spectra to Eq.(5) assuming different excitonic nonlinearities, it should be possible to determine the relative importance of different mechanisms of DX-IX interaction [45]. In the next Section, we show that at least one of the discussed mechanisms, namely energy shift of DX resonance, should produce a measurable nonlinear signal in realistic CQW structures.

III. IX-DX INTERACTION ENERGY

In this Section we estimate the strength of DX-IX Coulomb interaction in a typical CQW structure. Following the approach of [23–25] we use the Hartree-Fock and effective mass approximations to find matrix elements of the Coulomb interaction Hamiltonian. Our objective is to calculate the energy shifts of the bright DX levels $E_e^{\pm 1}$ and $E_h^{\pm 1}$ induced in the first order by the population of both bright ($n_I^{\pm 1}$) and dark ($n_I^{\pm 2}$) IX states. We also give estimations for IX-IX interaction energy within the same model, to compare with the PL line-shifts observed experimentally and with existing theoretical results.

We operate with a wavefunction of a single 1s-exciton characterized by a center of mass wave vector \mathbf{Q} with decoupled translational motion in the QW plane, electron and hole motion along z axis and relative motion of electron and hole:

$$\Psi_{\mathbf{Q}}(\boldsymbol{\rho}, z_{el}, z_{hh}) = \frac{1}{\sqrt{S}} \exp(i\mathbf{Q}\mathbf{R}_{c.m.}) \Psi_z(z_{el}, z_{hh}) \Psi_{\boldsymbol{\rho}}(\boldsymbol{\rho}), \quad (7)$$

where $\mathbf{R}_{c.m.} = (m_{el}\mathbf{r}_{el}^{\parallel} + m_{hh}\mathbf{r}_{hh}^{\parallel})/(m_{el} + m_{hh})$, $\boldsymbol{\rho} = \mathbf{r}_{el}^{\parallel} - \mathbf{r}_{hh}^{\parallel}$, $\mathbf{r}_{el, hh}^{\parallel}$ are electron and hole radius vector projections on the CQW plane, $m_{el, hh}$ are electron and hole in-plane effective masses. Relative motion part of this wavefunction $\Psi_{\rho}(\boldsymbol{\rho})$ for both DXs and IXs can be found from the solution of a 2D radial Schroedinger equation [41] or using the variational approach with the trial function of the form [25]:

$$\Psi_{\rho}(\boldsymbol{\rho}) = \frac{1}{\sqrt{2\pi b(b+r_0)}} \exp\left(\frac{-\sqrt{\rho^2 + r_0^2} + r_0}{2b}\right), \quad (8)$$

with r_0 and b as variational parameters. The corresponding mean square of in-plane radius for this exciton wavefunction is given by:

$$p^2 = \frac{2b}{b+r_0}(r_0^2 + 3br_0 + 3b^2). \quad (9)$$

Figure 3 (a) shows the ψ_{ρ} parameters p , b and r_0 as a function of QWs separation d , as obtained from the vari-

ational procedure. In the limiting case of $d = 0$, Eq. (9) coincides with the exact solution for the in-plane radius of the DX wavefunction with $r_0 = 0$ and $b = a_B/4$. When the separation between QWs increases, the in-plane extension of the IX wavefunction grows sublinearly. The wave function in z-direction in the limit of two infinitely thin QWs reads:

$$\Psi_z^{e(h)} = \delta(z_{el} - Z_{e(h)})\delta(z_{hh} - Z_{e(h)}),$$

for DX state, and for IX state

$$\Psi_z^I = \delta(z_{el} - Z_e)\delta(z_{hh} - Z_h),$$

where $Z_{e(h)}$ are the QW coordinates in the growth direction.

In Born approximation, the renormalization of DX and IX energies induced by the presence of a thermalized IX gas, is governed by the Coulomb exciton-exciton interaction operator.

$$\widehat{V} = \frac{e^2}{\epsilon} \left[\frac{1}{|\mathbf{r}_{el} - \mathbf{r}'_{el}|} + \frac{1}{|\mathbf{r}_{hh} - \mathbf{r}'_{hh}|} - \frac{1}{|\mathbf{r}_{el} - \mathbf{r}'_{hh}|} - \frac{1}{|\mathbf{r}_{hh} - \mathbf{r}'_{el}|} \right] \quad (10)$$

	$ e \downarrow \uparrow (+1)\rangle$	$ e \uparrow \downarrow (-1)\rangle$	$ h \downarrow \uparrow (+1)\rangle$	$ h \uparrow \downarrow (-1)\rangle$
$I \uparrow \uparrow (+2)$	0	V_{exch}^{D-1}	V_{exch}^{D-1}	0
$I \downarrow \uparrow (+1)$	V_{exch}^{D-1}	0	V_{exch}^{D-1}	0
$I \uparrow \downarrow (-1)$	0	V_{exch}^{D-1}	0	V_{exch}^{D-1}
$I \downarrow \downarrow (-2)$	V_{exch}^{D-1}	0	0	V_{exch}^{D-1}

TABLE I: Matrix elements contributing to the interaction of four possible IX spin states with bright DX states. Indices e , h and I refer to DX in electron and hole QWs and IX states, direction of arrows defines electron ($\uparrow\downarrow$) and hole ($\uparrow\downarrow$) angular momentum projection.

	$I \downarrow \uparrow (+1)$	$I \uparrow \downarrow (-1)$
$I \uparrow \uparrow (+2)$	$V_{\text{dir}}^{I-1} + V_{\text{exch}}^{I-1}$	$V_{\text{dir}}^{I-1} + V_{\text{exch}}^{I-1}$
$I \downarrow \uparrow (+1)$	$2(V_{\text{dir}}^{I-1} + V_{\text{exch}}^{I-1})$	V_{dir}^{I-1}
$I \uparrow \downarrow (-1)$	V_{dir}^{I-1}	$2(V_{\text{dir}}^{I-1} + V_{\text{exch}}^{I-1})$
$I \downarrow \downarrow (-2)$	$V_{\text{dir}}^{I-1} + V_{\text{exch}}^{I-1}$	$V_{\text{dir}}^{I-1} + V_{\text{exch}}^{I-1}$

TABLE II: Matrix elements contributing to the interaction of four possible IX spin states with bright IX states. Direction of arrows defines electron ($\uparrow\downarrow$) and hole ($\uparrow\downarrow$) angular momentum projection.

Here ϵ is material permittivity, e is the electron charge.

The shifts of DXs and IXs energy levels are simply the matrix elements of the Coulomb exciton-exciton interaction operator over two-exciton wavefunctions. These wavefunctions are obtained by antisymmetrization of the product of two single-exciton ground state ($Q = 0$) wavefunctions with respect to the permutation of either electrons or holes. In the general case of two excitons with spin projections on z -axis S, S' , corresponding to electron spin projections s_e, s'_e and heavy hole angular momentum projections j_h, j'_h this average has the following form [23]:

$$V_{SS'} = V_{\text{dir}} + \delta_{SS'} V_{\text{exch}}^X + \delta_{s_e s'_e} V_{\text{exch}}^{el} + \delta_{j_h j'_h} V_{\text{exch}}^{hh}, \quad (11)$$

where δ_{ij} is the Kronecker delta operator. The first term

V_{dir} is the direct Coulomb term which corresponds to the classical electrostatic interaction between the two excitons. V_{exch}^X is the term describing the simultaneous exchange of the two identical electrons and the two identical holes between two excitons. The third term V_{exch}^{el} is the term due to the electron-electron exchange, while V_{exch}^{hh} is the analogous contribution arising from the hole-hole exchange. In the limit of zero transferred momentum $V_{\text{dir}} = V_{\text{exch}}^X$ and $V_{\text{exch}}^{el} = V_{\text{exch}}^{hh}$ [23, 25].

Table I provides a convenient visual representation of all the interaction terms in Eq. (11). Along the vertical axis all IX spin states are listed. Four columns show the matrix elements responsible for their interaction with a pair of bright excitons in each QW. Mutual orientation of electron and hole spin in each exciton state is shown by arrows. Analogous representation of interactions be-

tween all four IX spin states and bright IX states are given by Table II.

For IX-DX interaction it can be shown that $V_{\text{dir}} = V_{\text{exch}}^X = 0$ due to the absence of stationary dipole moment for DXs and the assumed zero overlap of DX and IX wavefunctions. Therefore energy shifts of DXs due to IXs are governed by just one carrier exchange matrix element $V_{\text{exch}}^{el} = V_{\text{exch}}^{hh} \equiv V_{\text{exch}}^{\text{D-I}}$. As can be seen from Table 1, carrier exchange interaction for bright IXs is only possible with DXs with the same spin in both QWs, while DXs interacting with dark IXs have different spin projection signs in left and right QWs.

In the case of IX-IX interaction direct Coulomb term does not vanish in the Born approximation due to the oriented dipole moments of IXs and energy shifts of IXs are expressed in terms of two interaction constants $V_{\text{dir}} = V_{\text{exch}}^X = V_{\text{dir}}^{\text{I-I}}$ and $V_{\text{exch}}^{el} = V_{\text{exch}}^{hh} \equiv V_{\text{exch}}^{\text{I-I}}$. Direct Coulomb term is spin independent and enters every line in Table 1, while carrier exchange between two IXs is only possible if either electrons or holes have the same spin projections.

Two IXs with both electrons and holes having the same spin projections can also exchange them simultaneously. This gives factor 2 before $V_{\text{dir}}^{\text{I-I}}$ in corresponding cells of Table I.

Using the Table I, one can write the expressions for the DX and IX energy shifts, induced by the IX population. The bright DXs energy shifts depend on the population of the IXs with different spin projections on the growth axis as:

$$\delta E_e^\pm = V_{\text{exch}}^{\text{D-I}}(n_I^{\pm 1} + n_I^{\mp 2}), \quad \delta E_h^\pm = V_{\text{exch}}^{\text{D-I}}(n_I^{\pm 1} + n_I^{\mp 2}). \quad (12)$$

Energy shifts of bright IXs are related to IXs populations in a similar way (see Table II):

$$\delta E_I^\pm = (V_{\text{dir}}^{\text{I-I}} + V_{\text{exch}}^{\text{I-I}})(n_I^{+2} + n_I^{-2}) + 2(V_{\text{dir}}^{\text{I-I}} + V_{\text{exch}}^{\text{I-I}})n_I^{\pm 1} + V_{\text{dir}}^{\text{I-I}}n_I^{\mp 1} \quad (13)$$

Listed interaction constants are the matrix elements of interaction operator (11):

$$\begin{aligned} V_{\text{exch}}^{\text{D-I}} &= \int d^3\mathbf{r}_{el} d^3\mathbf{r}_{hh} d^3\mathbf{r}'_{el} d^3\mathbf{r}'_{hh} \Psi_0^{\text{D}}(\mathbf{r}_{el}, \mathbf{r}_{hh}) \Psi_0^{\text{I}}(\mathbf{r}'_{el}, \mathbf{r}'_h) \widehat{V}(\mathbf{r}_{el}, \mathbf{r}_{hh}, \mathbf{r}'_{el}, \mathbf{r}'_{hh}) \Psi_0^{\text{D}}(\mathbf{r}'_{el}, \mathbf{r}_{hh}) \Psi_0^{\text{I}}(\mathbf{r}_{el}, \mathbf{r}'_{hh}), \\ V_{\text{dir}}^{\text{I-I}} &= \int d^3\mathbf{r}_{el} d^3\mathbf{r}_{hh} d^3\mathbf{r}'_{el} d^3\mathbf{r}'_{hh} \Psi_0^{\text{I}}(\mathbf{r}_{el}, \mathbf{r}_{hh}) \Psi_0^{\text{I}}(\mathbf{r}'_{el}, \mathbf{r}'_h) \widehat{V}(\mathbf{r}_{el}, \mathbf{r}_{hh}, \mathbf{r}'_{el}, \mathbf{r}'_{hh}) \Psi_0^{\text{I}}(\mathbf{r}_{el}, \mathbf{r}_{hh}) \Psi_0^{\text{I}}(\mathbf{r}'_{el}, \mathbf{r}'_{hh}), \\ V_{\text{exch}}^{\text{I-I}} &= \int d^3\mathbf{r}_{el} d^3\mathbf{r}_{hh} d^3\mathbf{r}'_{el} d^3\mathbf{r}'_{hh} \Psi_0^{\text{I}}(\mathbf{r}_{el}, \mathbf{r}_{hh}) \Psi_0^{\text{I}}(\mathbf{r}'_{el}, \mathbf{r}'_h) \widehat{V}(\mathbf{r}_{el}, \mathbf{r}_{hh}, \mathbf{r}'_{el}, \mathbf{r}'_{hh}) \Psi_0^{\text{I}}(\mathbf{r}'_{el}, \mathbf{r}_{hh}) \Psi_0^{\text{I}}(\mathbf{r}_{el}, \mathbf{r}'_{hh}). \end{aligned} \quad (14)$$

While $V_{\text{dir}}^{\text{I-I}}$ can be found analytically [25], $V_{\text{exch}}^{\text{I-I}}$ and $V_{\text{exch}}^{\text{D-I}}$ should be calculated numerically using *e.g.* Monte-Carlo integration method. The result of matrix elements calculation by the Monte Carlo method is shown in Figure 3 (b) in the units of Ra_B^2 , where R and a_B are bulk exciton Rydberg energy and Bohr radius, respectively. One can see, that $V_{\text{exch}}^{\text{D-I}}$ almost does not depend on the separation between the QWs (dashed-dotted line). In contrast, both $V_{\text{exch}}^{\text{I-I}}$ (solid line) and $V_{\text{dir}}^{\text{I-I}}$ (dashed line) terms increase in absolute value with increasing distance between QWs, but have different signs. This result is in a good agreement with the calculations of Refs. [23, 25].

To further check the validity of this approach, it is instructive to calculate using Eqs. (12)-(13) the PL shifts of IX and DX lines in a typical CQW structure. We consider the situation where most of IXs are depolarized, so that energy shifts of light emitting states should be averaged over IX spin projections. This gives:

$$\begin{aligned} \delta E_e &= \delta E_h = \frac{1}{2} V_{\text{exch}}^{\text{D-I}} n_I \\ \delta E_I &= \left(\frac{5}{4} V_{\text{dir}}^{\text{I-I}} + V_{\text{exch}}^{\text{I-I}} \right) n_I, \end{aligned} \quad (15)$$

where n_I is the total density of IXs. The resulting energy shifts are shown in Figure 3 (c) for unitary IX density $n_I = a_B^{-2}$. Note that the shifts are obtained assuming negligible tunnel coupling between QWs and is incorrect in the vicinity of $d = 0$, where transition from weak to strong tunnel coupling occurs. In the latter case DX PL shift is twice higher. One can see, that for a given density of IX excitons, the PL shift of IX line exceeds the DX line shift. This difference dramatically enhances with increasing separation between QWs. For IXs densities $\sim 10^{10} \text{ cm}^{-2}$ and $d \sim 10 \text{ nm}$, DX and IX PL shifts are of the order of 0.1 meV and 1 meV respectively. This is consistent with the experimental observations [26].

We can now write down the expressions for both Kerr rotation and photoinduced reflectivity in the vicinity of each DX resonance. Substituting Eq.(12) into Eq.(6) with $E_{e(h)}$ as ξ we relate these signals to the IX populations:

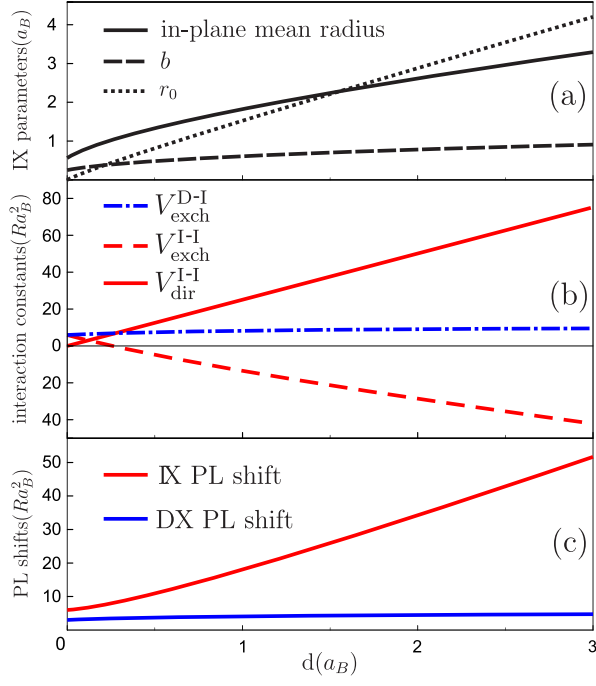


FIG. 3: (a) Parameters of the IX wave function obtained via variational procedure and the resulting in-plane radius. (b) Interaction constants computed by Monte-Carlo method. DX-IX carrier exchange constant V_{exch}^{D-I} (blue dot-dashed line), IX-IX carrier exchange constant V_{exch}^{I-I} (red dashed line) and direct or exciton exchange interaction constant V_{dir}^{I-I} (red solid line). (c) PL shifts of IX and DX lines calculated from Eqs. 15.

$$\begin{aligned}
 \delta\theta_e &= \frac{2n}{n^2-1} V_{\text{exch}}^{D-I} \text{Im}\{S_e\} [n_I^{+1} - n_I^{-1} + n_I^{+2} - n_I^{-2}] \\
 \delta\theta_h &= \frac{2n}{n^2-1} V_{\text{exch}}^{D-I} \text{Im}\{S_h\} [n_I^{+1} - n_I^{-1} - n_I^{+2} + n_I^{-2}] \\
 \delta R_e &= \frac{4n(1-n)}{(n+1)^3} V_{\text{exch}}^{D-I} \text{Re}\{S_e\} \sum_s n_I^s \\
 \delta R_h &= \frac{4n(1-n)}{(n+1)^3} V_{\text{exch}}^{D-I} \text{Re}\{S_h\} \sum_s n_I^s \quad (16)
 \end{aligned}$$

where $s = -2, -1, +1, +2$ numerates IX spin projections and the complex values between the braces are defined by:

$$S_{e(h)}(\omega) = e^{2ikl} \frac{\partial r_{\text{QW}}}{\partial E_{e(h)}} \quad (17)$$

Numerical application of these formula for IXs densities $\sim 10^{10} \text{ cm}^{-2}$, $d \sim 10 \text{ nm}$ and 100 % spin polarization of IXs, gives for both photoinduced differential reflectivity and Kerr rotation angle the values of the order of 10^{-2} . This allows predicting a measurable nonlinear signal in differential reflectivity and Kerr rotation even for weakly spin polarized IXs. Moreover, measurement of

Kerr rotation at both DX resonances, E_e and E_h , allows for determination of spin polarization degree of dark and bright IX separately:

$$n_I^{+1} - n_I^{-1} \sim \delta\theta_e + \delta\theta_h, \quad n_I^{+2} - n_I^{-2} \sim \delta\theta_e - \delta\theta_h, \quad (18)$$

as well as for determination of the total density of IXs:

$$n_I^{+1} + n_I^{-1} + n_I^{+2} + n_I^{-2} \sim \delta R_e \sim \delta R_h \quad (19)$$

Note, that the determination of dark IX polarization degree is only possible for the asymmetric CQW structure, where $|E_e - E_h| \gg \Gamma$, and two resonances at direct transitions provide independent signals. In symmetric CQWs $\delta E_e^\pm = \delta E_h^\pm$, which means that only total IXs density and polarization of bright IXs can be determined, while polarization of dark IXs remains hidden in this case.

In principle, the same effects may be observed at the IX transition frequency, although its magnitude is proportional to the radiative decay Γ_0 entering Eq.(1), which decays exponentially for IX resonance with separation of QWs. Indeed, in the IX resonance case, the integrand of Eq.(2) describes vanishing tails of the electron(hole) wavefunction in the hole(electron) QW. Substituting Eq.(13) into Eq.(6) in a similar manner yields the following expressions:

$$\begin{aligned}
 \delta\theta_I &= \frac{2n}{n^2-1} (V_{\text{dir}}^{I-I} + 2V_{\text{exch}}^{I-I}) \text{Im}\{S_I\} [n_I^{+1} - n_I^{-1}] \\
 \delta R_I &= \frac{4n(1-n)}{(n+1)^3} \left(\frac{3}{2} V_{\text{dir}}^{I-I} + V_{\text{exch}}^{I-I} \right) \text{Re}\{S_I\} [n_I^{+1} + n_I^{-1}] + \\
 &\quad + \frac{4n(1-n)}{(n+1)^3} (V_{\text{dir}}^{I-I} + V_{\text{exch}}^{I-I}) \text{Re}\{S_I\} [n_I^{+2} + n_I^{-2}]. \quad (20)
 \end{aligned}$$

where S_I is defined in the same manner as in Eq.(17).

Equations (16) and (20) form a closed non-degenerate system of linear equations on IXs spin state occupancies n_I^s , therefore measurements of nonlinear effects on both DX and IX transition frequencies in asymmetric CQWs allow for resolving all spin components of IXs system. In particular, bright and dark states populations can be resolved.

IV. SPIN DENSITY MATRIX MODEL

In this section, we shall specifically describe the time-resolved optically induced reflectivity and Kerr rotation in CQWs. The proposed formalism is similar to the formalism which was developed and successfully applied to QW microcavities in Ref. [27]. In this type of experiment short and circularly polarized pump pulse is tuned to direct resonance and creates DXs with certain spin. Short living DXs either relax into IX state or recombine, leaving a partially polarized IX system. Linearly polarized probe pulses, also set to the DX transition frequency

and weak comparing to the pump, act as analyzers of the current exciton density and polarization.

We use density matrix formalism to model the dynamics of a system containing both DXs and IXs between pump and probe pulses arrival. The state of the system can be conveniently described by a 16x16 density matrix with elements denoted as $\rho_{e,h,e',h'}^{s,s'}$, where $e, h, e', h' = 0, 1$ indicate the positions of electron and hole (0 or 1 for the electron or hole QW, respectively), $s, s' = -2, -1, +1, +2$ is the exciton spin state. This basis is convenient for the description of the electron and hole tunneling which converts DXs to IXs.

The initial conditions for the density matrix are governed by pump polarization and frequency. In the considered case of circularly polarized pumping only diagonal elements of initial density matrix $\rho_{e,h,e,h}^{s,s}$, with $s = \pm 1$ for σ^\pm pump helicity, are nonzero. Furthermore, if CQWs are asymmetric, DXs in both QWs can be pumped independently, so that only one diagonal component of the initial density matrix is nonzero, $\rho_{0,0,0,0}^{\pm 1, \pm 1}$ if the pump is tuned to the electron QW resonance, or $\rho_{1,1,1,1}^{\pm 1, \pm 1}$ if it is set to the hole QW resonance. In the case of symmetric CQWs both diagonal components with the same spin are

initially nonzero.

The evolution of the density matrix is generally described by a quantum Liouville equation:

$$i\hbar \frac{\partial \rho}{\partial t} = [\hat{H}, \rho] - i\hbar \hat{L}(\rho), \quad (21)$$

where the Hamiltonian \hat{H} describes coherent processes, while Lindblad superoperator \hat{L} describes all incoherent processes. We concentrate on the second term of Eq.(21) to model relaxational dynamics of the system. We shall account for: (i) tunneling and energy relaxation of electrons from the hole QW to the electron QW and of holes vice versa, described by the rates γ_e and γ_h respectively, (ii) radiative decay of bright DXs in both QWs $\Gamma_0^e = \Gamma_0^h = \Gamma_0^D$, the one of bright IXs Γ_0^I and corresponding nonradiative decays Γ^D and Γ^I , (iii) separate spin flips of electrons and holes, described by spin relaxation rates $\gamma_{e,s}$ and $\gamma_{h,s}$, and simultaneous electron and hole spin flips, its rate $\gamma_{X,s}$ is defined by electron-hole exchange and is only present for DXs since this mechanism is suppressed for IXs by spatial separation of electron and hole [17, 28, 29]. The Lindblad term reads:

$$\begin{aligned} L\left(\rho_{e,h,e',h'}^{s,s'}\right) = & \left[\left(\Gamma_0^D \delta_{e,h} \delta_{e',h'} + \Gamma_0^I \delta_{e,1-h} \delta_{e',1-h'} \right) (\delta_{s,+1} + \delta_{s,-1}) + \Gamma^D \delta_{e,h} \delta_{e',h'} + \Gamma^I \delta_{e,1-h} \delta_{e',1-h'} \right] \delta_{s,s'} \rho_{e,h,e',h'}^{s,s'} + \\ & \gamma_{es} \left[\delta_{s,+1} \delta_{s',+1} \rho_{e,h,e',h'}^{+2,+2} + \delta_{s,+2} \delta_{s',+2} \rho_{e,h,e',h'}^{+1,+1} + \delta_{s,-1} \delta_{s',-1} \rho_{e,h,e',h'}^{-2,-2} + \delta_{s,-2} \delta_{s',-2} \rho_{e,h,e',h'}^{-1,-1} \right] + \\ & \gamma_{hs} \left[\delta_{s,+1} \delta_{s',+1} \rho_{e,h,e',h'}^{-2,-2} + \delta_{s,-2} \delta_{s',-2} \rho_{e,h,e',h'}^{+1,+1} + \delta_{s,-1} \delta_{s',-1} \rho_{e,h,e',h'}^{+2,+2} + \delta_{s,+2} \delta_{s',+2} \rho_{e,h,e',h'}^{-1,-1} \right] + \\ & \delta_{e,h} \gamma_{Xs} \left[\delta_{s,+1} \delta_{s',+1} \rho_{e,h,e',h'}^{-1,-1} + \delta_{s,-1} \delta_{s',-1} \rho_{e,h,e',h'}^{+1,+1} + \delta_{s,+2} \delta_{s',+2} \rho_{e,h,e',h'}^{-2,-2} + \delta_{s,-2} \delta_{s',-2} \rho_{e,h,e',h'}^{+2,+2} \right] + \\ & + \gamma_e \delta_{e,0} \delta_{e',0} \rho_{1,h,1,h'}^{s,s'} + \gamma_h \delta_{h,1} \delta_{h',1} \rho_{e,0,e'}^{s,s'} \end{aligned} \quad (22)$$

Only the lowest in energy IX state, for which $e = 0$ and $h = 1$, is populated in our model via carrier tunneling and energy relaxation, while the one with $e = 1$ and $h = 0$ remains unpopulated and can be safely ignored. Neglecting nondiagonal elements of the density matrix, we reduce Eq.(21) to a linear matrix differential equation on the 12-component vector of DX and IX spin states populations $n_e^s = \rho_{0,0,0,0}^{s,s}$, $n_h^s = \rho_{1,1,1,1}^{s,s}$ and $n_I^s = \rho_{0,1,0,1}^{s,s}$:

$$\frac{d}{dt} \begin{pmatrix} n_e^s \\ n_h^s \\ n_I^s \end{pmatrix} = \begin{pmatrix} \hat{L}_D & 0 & 0 \\ 0 & \hat{L}_D & 0 \\ \gamma_h \hat{I} & \gamma_e \hat{I} & \hat{L}_I \end{pmatrix} \begin{pmatrix} n_e^s \\ n_h^s \\ n_I^s \end{pmatrix}, \quad (23)$$

where \hat{I} is the 4x4 identity matrix, \hat{L}_D and \hat{L}_I describe

decay and spin relaxation of DXs and IXs, respectively:

$$\hat{L}_D = \begin{pmatrix} -\Gamma^D & \gamma_{es} & \gamma_{hs} & \gamma_{Xs} \\ \gamma_{es} & -\Gamma_0^D - \Gamma^D & \gamma_{Xs} & \gamma_{hs} \\ \gamma_{hs} & \gamma_{Xs} & -\Gamma_0^D - \Gamma^D & \gamma_{es} \\ \gamma_{Xs} & \gamma_{hs} & \gamma_{es} & -\Gamma^D \end{pmatrix}, \quad (24)$$

$$\hat{L}_I = \begin{pmatrix} -\Gamma^I & \gamma_{es} & \gamma_{hs} & 0 \\ \gamma_{es} & -\Gamma_0^I - \Gamma^I & 0 & \gamma_{hs} \\ \gamma_{hs} & 0 & -\Gamma_0^I - \Gamma^I & \gamma_{es} \\ 0 & \gamma_{hs} & \gamma_{es} & -\Gamma^I \end{pmatrix} \quad (25)$$

The solution of Eq.(23) can be expressed using matrix exponent:

$$(n_e^s \ n_h^s \ n_I^s)^T = (n_e^s \ n_h^s \ n_I^s)^T \Big|_{t=0} \exp(t\hat{M}), \quad (26)$$

where \hat{M} is the 12x12 relaxation matrix given explicitly in the right part of (23).

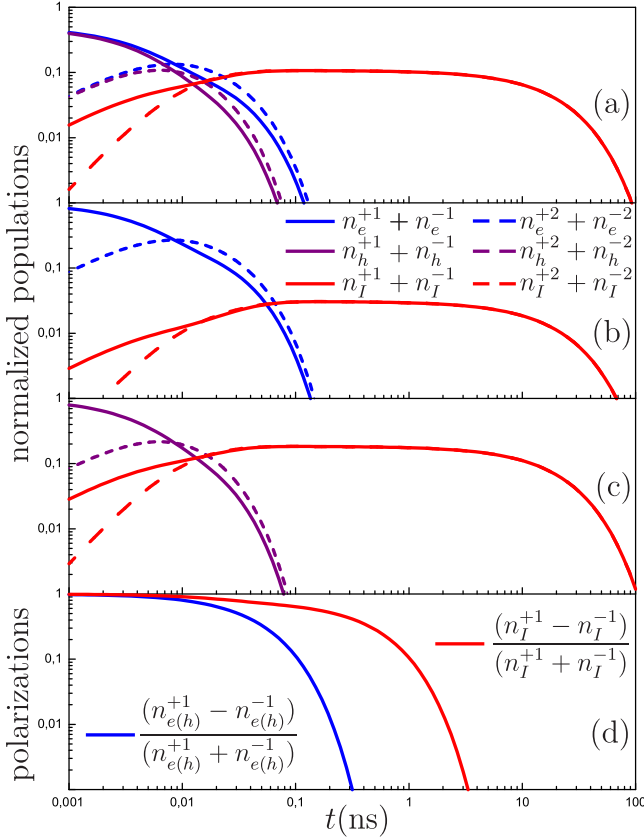


FIG. 4: Exciton relaxation dynamics in CQWs after a short circularly polarized pump pulse: (a) the normalised exciton populations in equally pumped symmetric CQWs; (b) the same for the pumping of an "electron" QW in asymmetric CQWs; (c) the same for the pumping of a "hole" QW in asymmetric CQWs; (d) DX and IX bright exciton polarization degrees. For all panels solid and dashed curves correspond to bright and dark states, respectively, blue and purple curves are related to DXs in electron and hole QWs, while red curves describe IXs. The parameters used in this calculation: $\gamma_h = (300 \text{ ps})^{-1}$, $\gamma_e = (30 \text{ ps})^{-1}$, $\Gamma^D \ll \Gamma_0^D = (100 \text{ ps})^{-1}$, $\Gamma^I \ll \Gamma_0^I = (10 \text{ ns})^{-1}$ [30], $\gamma_{es} = (1 \text{ ns})^{-1}$, $\gamma_{hs} = (10 \text{ ps})^{-1}$, $\gamma_{\chi_s} = (50 \text{ ps})^{-1}$ [31].

Substituting different initial conditions into Eq.(26) one can address various experimental scenarios. In the numerical analyses we focus on the three important cases: (i) DXs in both symmetric QWs are pumped simultaneously, (ii) CQWs are asymmetric, and we excite selectively DXs in the electron QW, in which case IXs are formed due to the hole tunneling, (iii) CQWs are asymmetric, and we excite selectively DXs in the hole QW, so that IXs are formed due to the electron tunneling. The cases (ii) and (iii) will be referred to as "electron QW pumping" and "hole QW pumping", respectively, to emphasize that in the case (ii) we optically create electrons in the same well where electrons of the lowest energy IXs are, while in the case (iii) we excite holes in the same well where the holes of the lowest energy IXs stay.

Figures 4(a,b,c) show populations of bright and dark DX and IX states as functions of time in the cases (i,ii,iii), respectively. In all cases the main features of IX and DX population dynamics are the same: the IXs population initially increases, while the DX population shows a fast decay due to the tunneling of electrons (ii), holes (iii), or both (i), and radiative recombination of DXs. At longer times, the IX population slowly decreases. Bright and dark exciton populations quickly equalize due to the hole spin relaxation. Note that maximum amount of IXs left after vanishing of DXs depends on the rate of conversion from DXs to IXs, which is different for listed cases. The conversion due to the electron tunneling is faster than one due to the hole tunneling because of the lighter electron than heavy hole effective mass in the structure growth direction. Figure 4(d) shows the dynamics of polarization degrees of bright DXs and IXs which is the same for all considered cases. The DX polarization induced by light quickly decays due to the γ_{χ_s} relaxation term describing simultaneous electron and hole spin-flips. IX polarization lives much longer as for IXs this term is inhibited. Interestingly, the fast depolarization of holes does not lead to the decay of polarization degree of either bright or dark excitons. Indeed, the transformations from +1(+2) to -1(-2) spin states or vice versa require both electron and hole spin flips. Fast hole spin flips, however, do lock bright and dark excitons polarization degrees to the same absolute values and different signs, which is why we only plot bright excitons polarization. We note also, that repolarization of DXs due to the effective Zeeman splitting induced by polarized IXs is negligibly small in the chosen range of parameters.

Figure 5 shows the differential reflectivities and Kerr rotation angles obtained for asymmetric (a,b) and symmetric (c) CQWs. These quantities are obtained using Eqs.(16) for the IXs contributions and the following expressions for the DXs contributions obtained within the same assumptions as in the Section III:

$$\begin{aligned} \delta\theta_{e(h)} &= \frac{4n}{n^2 - 1} V_{\text{exch}}^{\text{D-D}} \text{Im} \{S_{e(h)}\} \left[n_{e(h)}^{+1} - n_{e(h)}^{-1} \right] \\ \delta R_{e(h)} &= \frac{8n(1-n)}{(n+1)^3} V_{\text{exch}}^{\text{D-D}} \text{Re} \{S_{e(h)}\} \sum_s n_{e(h)}^s, \end{aligned} \quad (27)$$

where $V_{\text{exch}}^{\text{D-D}} = V_{\text{exch}}^{\text{I-D}}(d=0) = V_{\text{exch}}^{\text{I-I}}(d=0)$ are the exchange interaction constants calculated in [23]. In the present calculation, we have assumed equality of the interaction constants $V_{\text{exch}}^{\text{D-D}} = V_{\text{exch}}^{\text{I-D}}$, which is reasonable due to the weak dependence of $V_{\text{exch}}^{\text{I-D}}$ on the distance between the QWs d (see Fig. (3)). One can see that the Kerr rotation signal decays faster than the differential reflectivity signal, in general. This is not surprising as the Kerr effect is sensitive not only to the population of IXs but also to their spin polarization, which decays faster than population. There are two time-scales in the Kerr signal corresponding to the hole and electron spin relax-

ation times. In the case of asymmetric CQWs both reflectivity and Kerr signals are initially much stronger at the exciton resonance in the pumped QW, while at the characteristic time-scale of the tunneling transfer the reflectivity signals from both wells become comparable. The Kerr signal is always stronger in the electron QW than in the hole QW as the electron spin relaxation time is much longer than the hole spin relaxation time. The dynamics of Kerr rotation and differential reflectivity gives a direct access to DX and IX spin relaxation and recombination times, but also to the electron and hole spin relaxation and tunneling times.

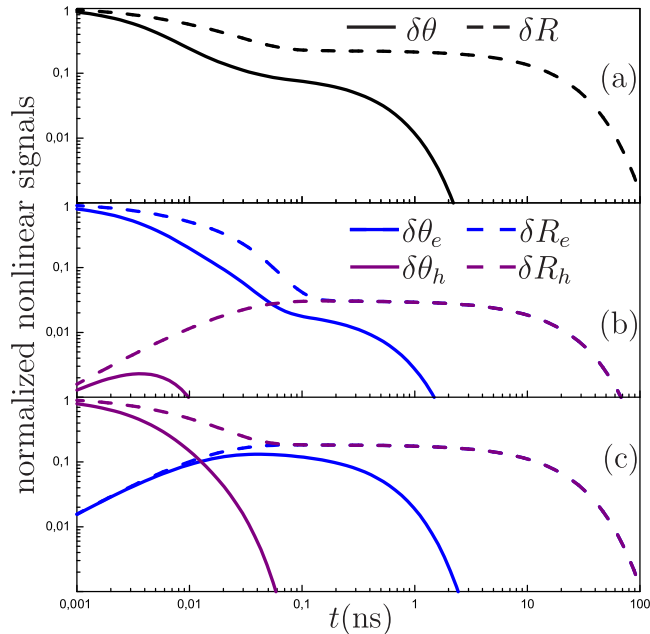


FIG. 5: Calculated dynamics of the photoinduced reflectivity (dashed curves) and Kerr rotation (solid curves) signals in CQWs after a short circularly polarized pump: (a) symmetric CQWs, both QWs are pumped (b) asymmetric CQWs, electron QW pumping (c) asymmetric CQWs, hole QW pumping. Blue and purple lines describe signals on electron and hole QWs resonant frequencies respectively, black curves describe folded signals from both symmetric CQWs. Parameters of calculation are the same as in Figure 4.

V. CONCLUSION.

We have shown that time-resolved pump-probe experiments offer new possibilities for studies of indirect excitons in coupled quantum well structures. To circumvent the problem of vanishing oscillator strength of IX state, we propose to detect the IX population and spin polarization via modifications of DX resonance properties. Three

different types of nonlinearities due to DX-IX interactions can be identified. Namely, DX resonance can shift in energy, change of its oscillator strength and/or broadening. We have shown, that relative contribution of these three mechanisms in measured time-resolved Kerr rotation and reflectivity can be identified via spectral profile of the photoinduced signal.

The calculation of DX-IX interaction energy allows to predict measurable nonlinear signals in CQW structures. Moreover, in asymmetric CQW structures where two distinct DX resonances can be addressed, Kerr rotation may provide information on both bright and dark exciton spin density.

To go further, we built up the spin density matrix formalism accounting for both DX and IX dynamics, relevant for realistic pump-probe experiments. Kerr rotation and reflectivity measured as a function of pump-probe delay can be described by the model. Fitting the experimental data to the model should give direct access to DX and IX decay, electron and hole depolarization and tunneling times.

This work has been supported by the EU FP7 ITN INDEX.

-
- [1] Sen Yang, A. T. Hammack, M. M. Fogler, L. V. Butov, A. C. Gossard, *Phys. Rev. Lett.* **97**, 187402 (2006)
 - [2] A. High, J. R. Leonard, A. T. Hammack, M. M. Fogler, L. V. Butov, A. V. Kavokin, K. L. Campman, A. C. Gossard, *Nature* **483**, 584 (2012).
 - [3] M. Alloing, D. Fuster, Y. González, L. González, F. Dubin, arXiv:1210.3176
 - [4] A. A. High, A. T. Hammack, J. R. Leonard, Sen Yang, L. V. Butov, T. Ostatnický, M. Vladimirova, A. V. Kavokin, T. C. H. Liew, K. L. Campman, A. C. Gossard, *Phys. Rev. Lett.* **110**, 246403 (2013).
 - [5] D. V. Vishnevsky, H. Flayac, A. V. Nalitov, D. D. Solnyshkov, N. A. Gippius, G. Malpuech, *Phys. Rev. Lett.* **110**, 246404 (2013).
 - [6] A. B. Dzyubenko and A. L. Yablonskii, *Phys. Rev. B* **53**, 16355 (1996).
 - [7] K. Sivalertporn, L. Mouchliadis, A. L. Ivanov, R. Philp, and E.A. Muljarov, *Phys. Rev. B* **85**, 045207 (2012).
 - [8] L. V. Butov, A. C. Gossard, D. S. Chemla, *Nature* **418**, 751 (2002).
 - [9] A. T. Hammack, L. V. Butov, L. Mouchliadis, A. L. Ivanov, A. C. Gossard, *Phys. Rev. B* **76**, 193308 (2007).
 - [10] S. Schmitt-Rink, D. S. Chemla, D. A. B. Miller, *Advances in Physics* **38**, 89 (1989).
 - [11] S. A. Crooker, J. J. Baumberg, F. Flack, N. Samarth, and D. D. Awschalom, *Phys. Rev. Lett.* **77**, 2814 (1996).
 - [12] Robert W. Boyd, *Nonlinear Optics*, Academic Press (2003).
 - [13] E. L. Boyd, *Optical Spectroscopy of Semiconductor Nanostructures*, Alpha Science International, Ltd (2005).
 - [14] J. J. Baumberg, D. D. Awschalom, N. Samarth, H. Luo and J. K. Furdyna, *Phys. Rev. Lett.* **72**, 717 (1994).
 - [15] A. Malinowski, R. S. Britton, T. Grevatt, R. T. Harley,

- D. A. Ritchie and M. Y. Simmons, *Phys. Rev. B* **62**, 13034 (2000).
- [16] M. Poggio, G. M. Steeves, R. C. Myers, N. P. Stern, A. C. Gossard, and D. D. Awschalom, *Phys. Rev. B* **70**, 121305(R) (2004).
- [17] J. R. Leonard, Y. Y. Kuznetsova, Sen Yang, L. V. Butov, T. Ostatnický, A. Kavokin, A. C. Gossard, *Nano Lett.* **9**, 4204 (2009).
- [18] M. Combescot, M. N. Leuenberger, *Solid State Comm.*, **149**, 567 (2009).
- [19] F. Tassone, F. Bassani, and L. C. Andreani, *Phys. Rev. B* **45**(11), 6023–6030 (1992).
- [20] L. E. Vorobiev, E. L. Ivchenko, D. A. Firsov, V. I. Shalygin. *Optical Properties of Nanostructures*. Nauka, St. Petersburg (2001).
- [21] M. Glazov, *Fizika Tverdogo Tela*, **54**, 1, 3 (2012) (*Physics of the Solid State*, **54**, 1, 1 (2012))
- [22] H. Hoffmann, G. V. Astakhov, T. Kiessling, W. Ossau, G. Karczewski, T. Wojtowicz, J. Kossut, and L. W. Molenkamp, *Phys. Rev. B* **74**, 073407 (2006).
- [23] C. Ciuti, V. Savona, C. Piermarocchi, A. Quattropani, and P. Schwendimann, *Phys. Rev. B* **58**, 7926 (1998)
- [24] S. Ben-Tabou de-Leon, and B. Laikhtman, *Phys. Rev. B* **63**, 125306 (2001)
- [25] O. Kyriienko, E. B. Magnusson, I. A. Shelykh, *Phys. Rev. B* **86**, 115324 (2012)
- [26] L.V. Butov, A. Imamoglu, K.L. Campman, and A.C. Gossard, *Zh. Éksp. Teor. Fiz.* **119**, 301 (2001) [*JETP* **92**, 260 (2001)]; *ibid.* [**92**, 752 (2001)].
- [27] A. Brunetti, M. Vladimirova, D. Scalbert, M. Nawrocki, A. V. Kavokin, I. A. Shelykh, and J. Bloch, *Phys. Rev. B* **74**, 241101 (2006).
- [28] M. Z. Maialle, E. A. de Andrada e Silva, L. J. Sham, *Phys. Rev. B* **47**, 15 776 (1993).
- [29] G. Aichmayr, M. Jetter, L. Vina, J. Dickerson, F. Camino, and E. E. Mendez, *Phys. Rev. Lett.* **83**, 2433 (1999).
- [30] A. Alexandrou, J. A. Kash, E. E. Mendez, M. Zachau, J. M. Hong, T. Fukuzawa, Y. Hase, *Phys. Rev. B* **42**, 9225 (1990).
- [31] A. Vinattieri, J. Shah, T.C. Damen, D.S. Kim, L.N. Pfeiffer, M.Z. Maialle, L.J. Sham, *Phys. Rev. B* **50**, 10868 (1994)
- [32] S. Cronenberger, M. Vladimirova, S. V. Andreev, M. B. Lifshits, and D. Scalbert, *Phys. Rev. Lett.* **110**, 077403 (2013).
- [33] L. V. Butov, A. L. Ivanov, A. Imamoglu, P. B. Littlewood, A. A. Shashkin, V. T. Dolgoplov, K. L. Campman, A. C. Gossard, *Phys. Rev. Lett.* **86**, 5608 (2001).
- [34] Yu. E. Lozovik, V. I. Yudson, *Sov. Phys. JETP* **44**, 389 (1976).
- [35] T. Fukuzawa, S. S. Kano, T. K. Gustafson, T. Ogawa, *Surf. Sci.* **228**, 482 (1990).
- [36] J. Feldmann, G. Peter, E. O. Göbel, P. Dawson, K. Moore, C. Foxon, R. J. Elliott, *Phys. Rev. Lett.* **59**, 2337 (1987).
- [37] E. Hanamura, *Phys. Rev. B* **38**, 1228 (1988).
- [38] L. C. Andreani, F. Tassone, F. Bassani, *Solid State Commun.* **77**, 641 (1991).
- [39] L.V. Butov, V.D. Kulakovskii and A. Forchel, *Phys. Rev. B* **48**, 17933 (1993).
- [40] M. Combescot, R. Combescot, M. Alloing and F. Dubin, arXiv:1307.1256v1.
- [41] N. A. Gippius, A. L. Yablonskii, A. B. Dzyubenko, S. G. Tikhodeev, L. V. Kulik, V. D. Kulakovskii, and A. Forchel, *Journal of Applied Physics*, **83**, 5410 (1998)
- [42] We note that probing an exciton sub-system with a low oscillator strength using an exciton sub-system with a higher oscillator strength was earlier explored in the studies of indirect excitons by linear methods: the optically dark excitons with spin ± 2 [28] or with high momenta beyond the radiative zone [36–38] were probed via the energy shift and optical decay rate of bright indirect excitons (with spin ± 1 and momenta within the radiative zone), see e.g. [9, 33].
- [43] Dark DX states characterised by total spin ± 2 have zero oscillator strength and do not contribute to the reflectivity spectra
- [44] We note that exciton resonance frequency renormalization due to the interaction with the carriers at other levels was also studied for excitons in dense electron-hole magnetoplasma [39] and for bright and dark indirect excitons [40].
- [45] The Faraday rotation spectroscopy provides the same information as the Kerr rotation spectroscopy with the only difference in the detection geometry: the transmitted signal is studied in the Faraday configuration, while in Kerr configuration the reflected signal is detected.